American Journal of Engineering Research (AJER)
e-ISSN: 2320-0847 p-ISSN : 2320-0936
Volume-13, Issue-12, pp-23-34
www.ajer.org
Research Paper Open Access

An Evaluation of Predictive Modeling and Error Analysis for Physicochemical Characteristics of Gasoline-Bioethanol Blends in a Gasoline Engine

[1]Ogunsola A.D. [2]Alajede A. M, [3]Olafimihan E.O, [4]Sangotayo E.O*, [5]Aderibigbe A. A. & [6]Sulaiman A. O.

[1,2,3,4,5,] *Department of Mechanical Engineering, Ladoke Akintola University of Technology, Ogbomoso, Nigeria,*
[6] *Department of Aeronautics and Astronautics Engineering, Kwara State University, Malete, Kwara, Nigeria.,*
[*]*Corresponding author: eosangotayo@lautech.edu.ng*

ABSTRACT
The integration of bioethanol into gasoline blends has gained significant attention for improving engine performance and reducing environmental impacts. This study evaluated predictive modeling and error analysis of the physicochemical characteristics of gasoline-bioethanol blends (E0, E5, E10, and E15) in a four-stroke gasoline engine. The importance of optimizing blend ratios for efficiency and sustainability underscores the relevance of this research. The physicochemical characteristics, including cetane number, viscosity, density, carbon residue, and heating values, were measured using a data logger and analyzed across blend ratios ranging from 0% to 15%. Profiles of these characteristics were created to assess their relationship with bioethanol content. Predictive models were developed using SAS software, with R-squared and RMSE values evaluated as performance metrics to assess model accuracy and fitness.
The results indicate that the coefficient of performance (COP) demonstrated higher sensitivity to bioethanol content in the 0-10% range, stabilizing about10%, suggesting an optimal blend ratio of around 10%. Brake power efficiency decreased linearly with increasing bioethanol content due to the lower energy density of higher ethanol blends. However, the enhanced combustion efficiency of bioethanol compensated for some efficiency losses. Notably, the E10 blend achieved the highest brake power of 391.65 W, Model evaluation revealed robust predictive capabilities, with R-squared and RMSE values for COP at 0.964 and 0.585, respectively, and for braking thermal efficiency at 0.996 and 0.133, respectively. These metrics confirm the model's high accuracy and reliability in predicting engine performance characteristics across blend ratios. Future research should explore the impact of higher ethanol concentrations on engine durability and further optimization of bioethanol-gasoline formulations for enhanced sustainability and effectiveness.
Keywords: Predictive Modeling; Engine Performance; Error Analysis, Physicochemical, SAS, Bioethanol Blends

---

Date of Submission: 28-11-2024 Date of acceptance: 07-12-2024

I. INTRODUCTION

The increasing need for sustainable and eco-friendly energy sources has heightened the emphasis on renewable fuels such as bioethanol which was derived from biomass like corn, sugarcane, and cellulosic materials, provides a renewable substitute for fossil fuels. Combining bioethanol with gasoline diminishes greenhouse gas emissions and improves fuel characteristics, including octane rating, so enhancing engine performance. Gasoline-bioethanol mixtures, typically designated as E10 (10% ethanol) or E15 (15% ethanol), are already utilized worldwide, demonstrating the pragmatic potential of bioethanol in tackling energy and environmental issues [1]. The incorporation of ethanol modifies the physicochemical characteristics of gasoline, encompassing density, viscosity, energy content, and vapor pressure. These modifications affect combustion properties, engine efficiency, and emissions. Understanding and forecasting these alterations is essential for optimizing blend formulations to attain a balance among efficiency, performance, and environmental sustainability. Predictive modeling provides a robust method for understanding the intricate relationships

between fuel characteristics and engine performance. The predictive models can replicate the impact of ethanol concentration fluctuations on the physicochemical parameters of the mix using experimental data and sophisticated computational methods, Biodiesel is being utilized in a growing array of sectors as a clean energy source, as global demand for renewable energy rises and It can be directly blended with petroleum diesel and is extensively utilized in transportation, agricultural machinery, power generation equipment, and several other sectors. In recent years, numerous nations and areas have advanced the production and utilization of biodiesel via policy incentives and regulatory mandates to diminish reliance on fossil fuels and mitigate greenhouse gas emissions [,2,3].

Biodiesel has emerged as a highly viable alternative fuel among other renewable energy sources due to its renewability, environmental sustainability, and compatibility with existing diesel engines. Biodiesel is a fuel derived by the transesterification of vegetable oil, animal fat, or waste oil with alcohols (such as methanol or ethanol), primarily consisting of fatty acid methyl esters (FAMEs). In comparison to conventional petroleum diesel, biodiesel not only diminishes greenhouse gas emissions but also significantly lowers the emissions of carbon monoxide (CO), hydrocarbons (HC), and particle matter (PM), thus alleviating air pollution and enhancing environmental quality [5]. Globally, the utilization of biodiesel fosters agricultural and industrial advancement while significantly diminishing reliance on petrochemical fuels [6]. Nonetheless, notwithstanding the benefits exhibited by biodiesel in the environmental and energy sectors, numerous challenges persist in its practical implementation. The physicochemical qualities of biodiesel vary considerably based on the raw materials and production methods, which directly influence its performance in diesel engines [7]. The combustion characteristics, emission characteristics, and engine performance effects of biodiesel in engines also fluctuate based on the fuel content. Consequently, precise prediction of biodiesel characteristics and its efficacy in diesel engines is a primary emphasis of contemporary research [8].

The characteristics of biodiesel directly influence its efficacy in diesel engines. The physicochemical properties of biodiesel, including viscosity, density, heating value, and oxidation stability, influence not only the combustion efficiency of the fuel in the engine but also the engine's starting performance, fuel consumption, emission characteristics, and long-term reliability. The combustion process of biodiesel in diesel engine systems directly influences thermal efficiency, power production, and emissions. The elevated oxygen concentration in biodiesel enhances combustion efficiency and diminish HC and CO emissions [9]. This trait results in elevated nitrogen oxide (NOx) emissions. Consequently, in the optimal design of engines, it is essential to account for both the physicochemical qualities and combustion characteristics of the fuel. Robust predictive models must be developed to assess the comprehensive performance of biodiesel. Conventional research methodologies primarily derive the qualities of biodiesel from experimental measurements; however, this approach is both time-intensive and expensive, and it is also subject to specific experimental inaccuracies. [10]. With the advancement of computing technology and data science, predictive methodologies utilizing mathematical models and machine learning (ML) have become significant research domains. These approaches may swiftly forecast biodiesel characteristics by utilizing current experimental data, offering a solid scientific foundation for fuel research and application.

The creation of predictive models can significantly reduce trial time and costs while examining the effects of various raw materials and manufacturing methods on fuel performance, therefore optimizing production and enhancing fuel quality [11]. Prediction models utilizing linear regression, support vector machines (SVMs), and artificial neural networks (ANNs) can precisely forecast essential characteristics such as heating value, viscosity, and oxidation stability of biodiesel [12]. The utilization of these models allows researchers to comprehend the attributes of various biodiesel fuels, offering efficient instruments for fuel optimization design. Simultaneously, a growing contingent of researchers is employing data-driven methodologies to forecast the performance of biodiesel in engines. Through the analysis of extensive experimental data and model training, machine learning techniques elucidate the intricate nonlinear correlations between fuel characteristics and engine performance, resulting in very accurate forecasts. These methodologies offer novel insights into the research of biodiesel-engine interactions and provide substantial assistance in optimizing fuel mixtures and engine design.

Sangotayo et al. [13] formulated models that delineate the statistical correlation between operational parameters, including input and outlet temperatures as a function of local time, and response variables such as COP and EER. Regression analysis is a robust statistical instrument that allows researchers and engineers to create predictive models for comprehending and enhancing systems. Biodiesel, as a crucial renewable energy source, has substantial environmental advantages and application potential due to its renewability, reduced carbon dioxide emissions, and favorable biodegradability. Biodiesel research has advanced swiftly, with scholars consistently broadening the sources of raw materials, fuel blend compositions, and application contexts for biodiesel [14]. The efficacy of biodiesel fluctuates based on the raw materials utilized. Moreover, biodiesel is generally combined with diesel through the use of additives for practical application. Consequently, the characteristics of biodiesel blends and their efficacy in diesel engines are more intricate than those of other

alternative fuels. This present research focuses on the assessment of predictive modeling and error analysis for physicochemical characteristics of gasoline-bioethanol blends in a gasoline engine

II. MATERIALS AND METHODS

Materials and Equipment

This study utilized the following materials and components: a 35-liter Bed Side refrigeration system, a 0.5mm thick aluminum light sheet, automotive paint in Ash color, a 16-gauge electrode, a capillary tube, a hose, fiber, resin, wheels, bioethanol fuel (quantity and composition), and refrigerant (R134a).

Construction and Development of a Compartment

The bio-ethanol engine, automotive air conditioner, and vaccine storage are the three systems that constitute the compact refrigeration module. The automotive air conditioner is directly connected to the bio-ethanol generator. The refrigeration unit that is implemented is a modification of the original components of an automotive vapor-compression air-conditioning system, which consists of a compressor, condenser, expansion valve, and evaporator, as well as an oil chiller and oil separator. The movement of air streams facilitates the exchange of heat between the condenser and evaporator. The thermostatic type of expansion valve is implemented. The refrigerant for this investigation will be R-134a. The indoor coil, which serves as an evaporator, absorbs heat from the fan-driven air stream as the refrigerant passes through it, thereby delivering refrigeration. The refrigerant is introduced to the outdoor coil after compression, where it dissipates heat into an additional air stream. The automotive air conditioning system is capable of functioning in a refrigeration cycle.
A 4-stroke, single-cylinder gasoline engine with a power output of 5 to 10 horsepower was implemented. This engine supplied the mechanical energy necessary to operate the refrigeration compressor. Equation (1) determines the engine's I.C. brake output and Equation (2) determines the brake power, P_B.

$$PB = T\omega \qquad (1)$$

ω is the angular speed in radians per second (rad/sec.)

$$\text{But,} \quad \omega = \frac{2\pi N}{60}$$

$$\text{Thus,} P_B = 2\frac{\pi N}{60} \cdot T \qquad (2)$$

Equation 3 gives the expression for the brake thermal efficiency.

$$\eta_b = \frac{P_B}{mf \cdot CV} \qquad (3)$$

Where P_B is the brake power in watts, m_f is the mass flow rate of the fuel by this engine in kg/s, CV is the heating value used by this engine in J/kg.

Refrigeration System

Figure 1 displays the components of the refrigeration system, which includes a compressor, refrigerant, heat exchangers, and condenser. The refrigeration system is depicted in Figure 2 from the orthogonal and isometric perspectives such as from the front, end, and top views.

i. Refrigeration Compressor - a reciprocating compressor that is hermetically sealed and compatible with the engine's power output was chosen. The refrigerant's pressure and temperature were increased by compressing it with the compressor.
ii. Refrigerant - R134a, an environmentally benign refrigerant, was used to charge the system. This was charged by the system's specifications.
iii. Heat Exchangers - These were employed to transfer heat from the refrigerated chamber to the external environment.
iv. Condenser - A condenser that is air-cooled and has an adequate heat rejection capacity was employed. The purpose of this was to transfer heat from the refrigerant to the ambient air.
v. Evaporator - A fin-tube-type evaporator was implemented. This functioned to absorb heat from the refrigerated space.
vi. Thermostatic Expansion Valve (TXV): A Thermostatic Expansion Valve (TXV) was installed. This regulated the passage of refrigerant into the evaporator.
vii. Refrigeration Chamber: This is an insulated chamber with a volume of approximately 1-2 cubic meters that was employed. This functioned as the experiment's cooling compartment.

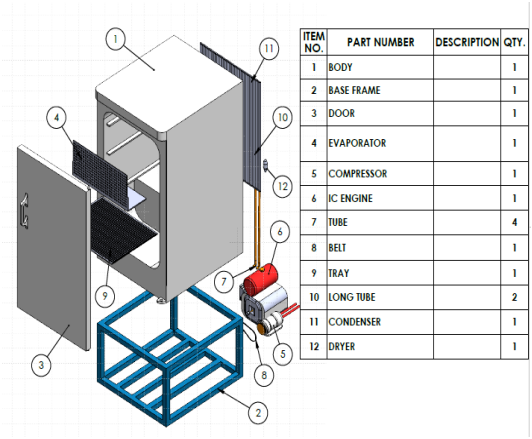

ITEM NO.	PART NUMBER	DESCRIPTION	QTY.
1	BODY		1
2	BASE FRAME		1
3	DOOR		1
4	EVAPORATOR		1
5	COMPRESSOR		1
6	IC ENGINE		1
7	TUBE		4
8	BELT		1
9	TRAY		1
10	LONG TUBE		2
11	CONDENSER		1
12	DRYER		1

Figure 1: Refrigeration System

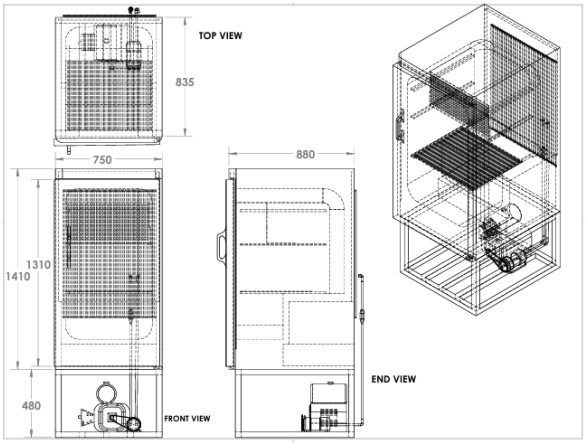

Figure 2: Orthogonal and Isometric View of the Refrigeration System

III. METHODOLOGY FOR SYSTEM ASSEMBLY

A suitable coupling of the belt drive system was implemented to establish a connection between the refrigeration compressor and the petroleum engine. The compressor discharge line was connected to the condenser intake using copper tubing. The expansion valve outlet was connected to the evaporator inlet, and the expansion valve inlet was connected to the condenser outlet. The evaporator output was reconnected to the compressor vacuum line. All connections were examined to ensure they a secured and leak-proof, they were examined. Vacuum pumps were implemented to evacuate the system, thereby eradicating any air and moisture. Subsequently, the refrigerant (R134a) was introduced into the system.

EVALUATION OF PERFORMANCE

The compressor vacuum and discharge pressures, temperatures at critical locations, refrigerant flow rate, and fuel consumption rate of the gasoline engine were monitored and recorded. The temperature and flow rate data that were obtained were analyzed to ascertain the cooling capacity of the system.
Coefficient of Performance (COP) was computed using Equation 4.

$$\text{COP} = \frac{\text{Cooling Capacity (kW)}}{\text{Engine Power Input (kW)}} \quad (4)$$

The Gasoline-driven refrigeration system's efficacy was assessed using the Coefficient of Performance (COP)

Data Collection

The data logger was utilized to collect data on temperature, pressure, and flow rate throughout the testing period. The cooling capacity, coefficient of performance (COP), and fuel efficiency were computed. Theoretical predictions were compared with experimental outcomes. The data was examined to discern trends, including the impact of engine strain on system performance.

Technique of model assessment

The correctness of the correlations was evaluated using two widely employed statistics metrics: Root Mean Square Error (RMSE) and Mean Absolute Bias Error (MABE). (MJ/m^2) for the regression model as presented in Eq.(5-7), [16,16,17]

$$MBE = \left[\sum \left(H_{i,c} - H_{i,m}\right)\right] / n \quad (5)$$

$$MABE = \left[\sum \left(\left|H_{i,c} - H_{i,m}\right|\right)\right] / n \quad (6)$$

$$RMSE = \left\{\left[\sum \left(H_{i,c} - H_{i,m}\right)^2\right] / n\right\}^{1/2} \quad (7)$$

The RMSE test offers insight into the short-term efficacy of correlations by facilitating a term-by-term comparison of the actual discrepancies between estimated and measured values; a smaller RMSE indicates a more precise estimate. A positive MBE indicates overestimation, whereas a negative number denotes underestimated by the model. A disadvantage of this approach is that an overestimation of one observation negates an underestimation of another, resulting in MBE values that demonstrate systematic error or bias, while RMSE reflects a non-systematic error [18]. The research assessed the correlations and regressions among the blend ratios, physicochemical properties, and performance parameters of the system The coefficient of determination (R^2) seeks to attain a value of 1, ideally reaching 100% to ensure greater accuracy and reliability in data modeling [19].

IV. RESULT AND DISCUSSION

Micro Cooling System Assembly Developed

Micro-cooling systems were developed to maintain the appropriate temperature for preservation. Figure 3 shows the developed micro-cooling system assembly and the assembly includes the insulated compartment, cooling unit, temperature control system, data logging and monitoring, evaporator outlet and blower motor with protective cover, condenser with fan, dryer, alternator, freezer compartment, base and base tire, vaccine tray, and working substance.

Micro-cooling systems reduce heat transfer from the outside via an enclosed compartment and the highest-quality thermal insulation materials utilized in this compartment maintain the internal temperature regardless of ambient conditions. The compartment's cooling technology was designed to keep the air temperature within the vaccine storage range. The energy-efficient cooling unit runs for a long time without using much power and a precise temperature control system with digital thermostats and sensors was also developed. These components continuously monitor the interior temperature to modify cooling output. This ensures that temperature fluctuations from the ideal range (2°C to 8°C) were obtained, maintaining reliable preservation conditions. The system logs data for the tracking of temperature changes to monitor vaccine storage.

The micro refrigeration system can run on AC mains and battery backup using a gasoline-bioethanol blend. Immunizations can be preserved in locations with intermittent energy, making them suitable for distant areas or emergencies. A crucial healthcare invention, the gasoline-driven vaccine refrigeration system (Figure 3), ensures appropriate vaccine storage and transportation. Its strong architecture and precise temperature management help preserve vaccine efficacy and public health and safety.

Figure 3: Assemblage of Gasoline-driven Refrigeration System

Physicochemical Properties of Gasoline-Bioethanol Blends

Figures 4 to 11 show that each physicochemical feature fluctuated as the volume fraction of ethanol in the combinations rose. The predictive models were developed using SAS software as presented in Figures 4 -14 with the corresponding coefficient of determination, $R^{2,}$ and its trends. The gasoline-bioethanol mixture increased density, viscosity, heating parameters, and specific gravity. Predictive models of the properties are shown on the plot and error analysis of models are evaluated as function MSE and RMSE.

Figure 4 shows octane numbers against blending ratios. Fuel mixtures with ethanol blends from 6% to 15% have higher octane ratings than those with 0 to 6%. At a 6% blend ratio, the minimum octane is 8°C. This helps reduce ringing in high-compression engines, which need higher-octane fuels. Ethanol burns cooler and consumes slower than gasoline, allowing for more regulated combustion. This improves the blend's effective octane rating, reducing pre-ignition and clanging.

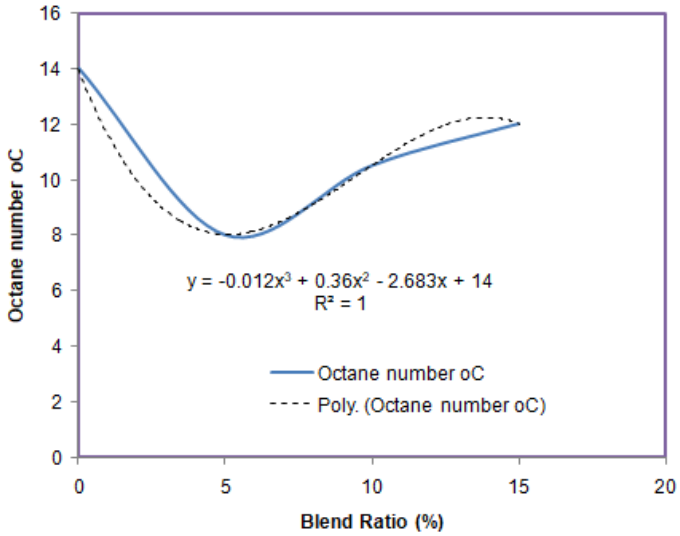

Figure 4: Trend of Octane Number against Blending Ratios

Figure 5 shows the link between blending ratios and centipoise viscosity at 20 °C. Viscosity rises from 0 to 6%, then drops as ethanol is added to gasoline, raising the blend ratio from 6% to 15%. At a 6% mix ratio, viscosity peaks at 14 centipoise. Additionally, ethanol is more viscous than petroleum. Blending increases fuel mixture viscosity (Figure 5). This change may affect engine combustion and fuel atomization. In cooler temperatures, ethanol may have higher fuel viscosity than pure gasoline, reducing engine performance and fuel delivery. At operational temperatures, viscosity may stabilize, but the compound will still be thicker than gasoline.

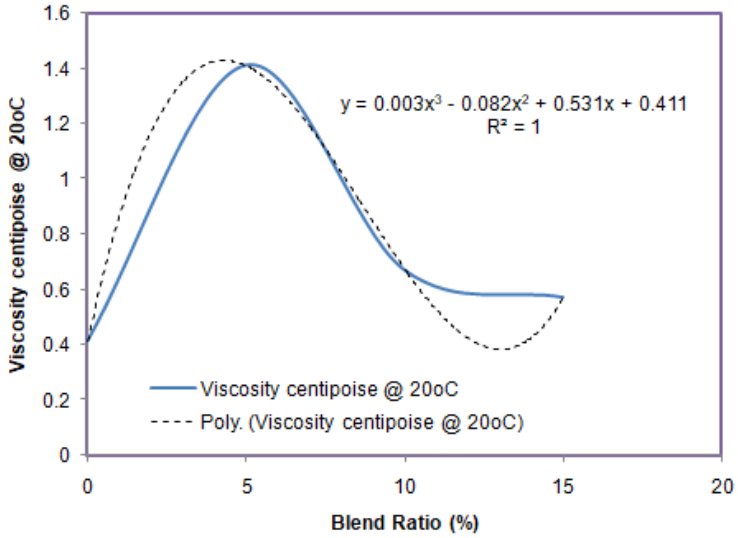

Figure 5: Trend of Viscosity centipoise @ 20 °C against Blend Ratio (%)

In Figure 6, Flashpoint is graphed against blending ratios. Ethanol blends with gasoline from 6% to 15% increase the fuel mixture's flashpoint. At 6% mix ratio, 25°C is the minimal flashpoint. Blended gasoline is less volatile than pure gasoline because its flash point rises. This can improve storage and handling safety. The addition of ethanol to gasoline should change its volatility. Ethanol reduces gasoline's lighter components' volatility, raising the blend's flash point. This change may lessen vapor lock and improve high-temperature safety.

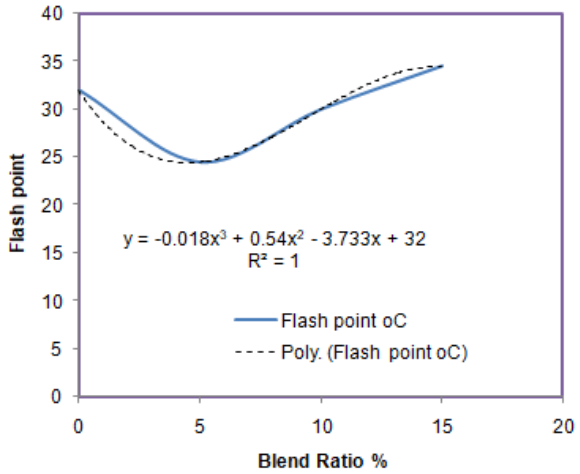

Figure 6: Trend of Flashpoint versus Blending Ratios

Density-blending ratio correlation is shown in Figure 7. Density increases from 0 to 6%, then declines when ethanol is combined with gasoline, boosting the blend ratio from 6% to 15%. At 6%, the density reaches 0.89 kg/L. Ethanol reduces gasoline density (Figure 7). Engine fuel supply and combustion may be affected by density reduction. The fuel density reduces as ethanol content increases. This may vary fuel volumetric flow rate, influencing engine performance and efficiency. The combination's density increased.

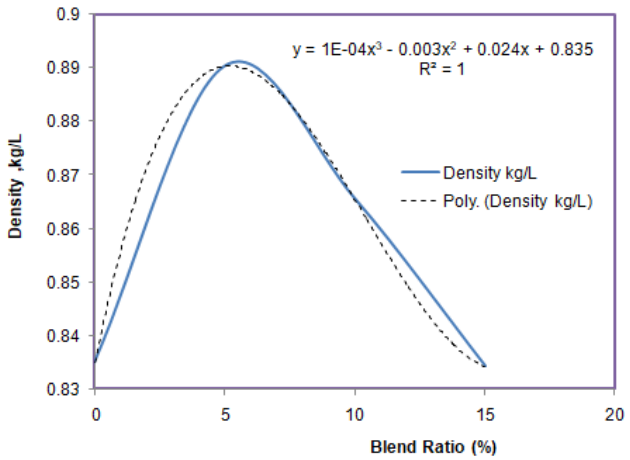

Figure 7: Trend of Density (kg/L) versus Blend Ratio (%)

Figure 8 shows the carbon residue-blending ratio graph. The carbon residue in the fuel mixture reduces from 0% to 10% but increases when 10% to 15% ethanol is added to gasoline. The minimum carbon residue is 74% at a 10% mixing ratio. Ethanol has less carbon and more oxygen than gasoline, which reduces carbon residue at lower blend ratios, but gasoline's high carbon content persists at lower ethanol concentrations. The blend with 10% ethanol has the lowest Carbon residue (74%), indicating excellent mixing. However, adding more complicated compounds may increase Carbon residue. Lower carbon residue reduces particulate matter and CO_2 emissions, while optimum blending ratios boost engine efficiency and reduce maintenance.

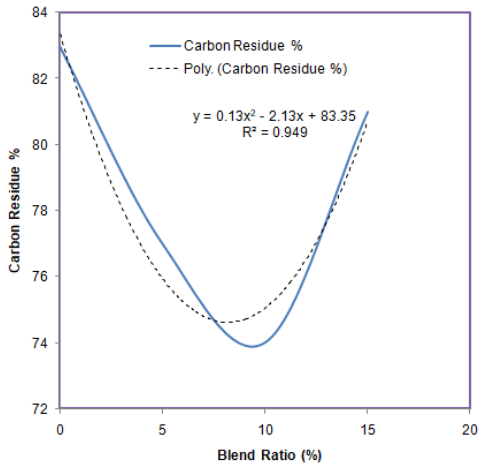

Figure 8: Trend of Carbon residue versus Blend Ratio (%)

Blending ratios and Specific Gravity (SG) are shown in Figure 9. Specific gravity rises from 0 to 6%, then drops when ethanol is added to gasoline, raising the blend ratio from 6% to 15%. At 6% blend ratio, specific gravity peaks at 0.85. Specific gravity affects fuel density, viscosity, and combustion properties. Ideal blending ratios increase engine efficiency, power output, and emissions, and understanding SG-blend ratio connections helps refine fuel specifications. Suboptimal interactions between ethanol and gasoline at high concentrations, the surplus of ethanol increasing volume and decreasing density, and molecular arrangements that affect mixture density may reduce specific gravity beyond the 6% blend ratio.

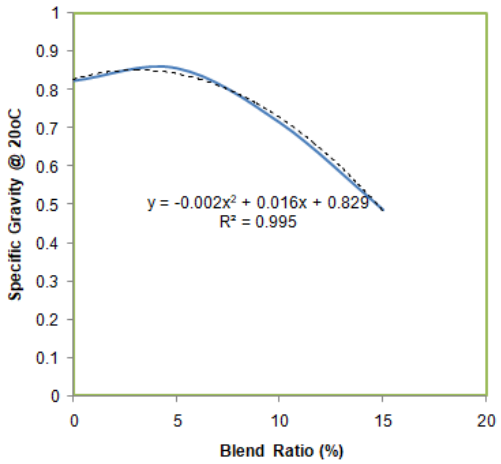

Figure 9: Trend of Specific Gravity @ 20oC versus Blend Ratio (%)

Figure 10 shows how mixing ratios affect the pour point. As the blend ratio rises from 0% to 15%, the fuel mixture's pour point fluctuates. The pour point peaks at 8ºC at a 10% blend ratio. It shows that ethanol's lower viscosity and higher volatility affect the blend's pour point. At 0-5% ethanol, gasoline dominates the combination. Ethanol and gasoline molecules interact to raise the pour point (5-10%). The blend's pour point (8°C) at 10% ethanol indicates optimal mixing. Over 10% pour point decreases: The pour point is decreased by adding 10-15% ethanol, which may disrupt molecular connections. The pour point affect gasoline flowability, especially in cooler conditions. Optimized blending ratios ensure engine reliability, while Pour point-blend ratio relationships guide fuel storage and management.

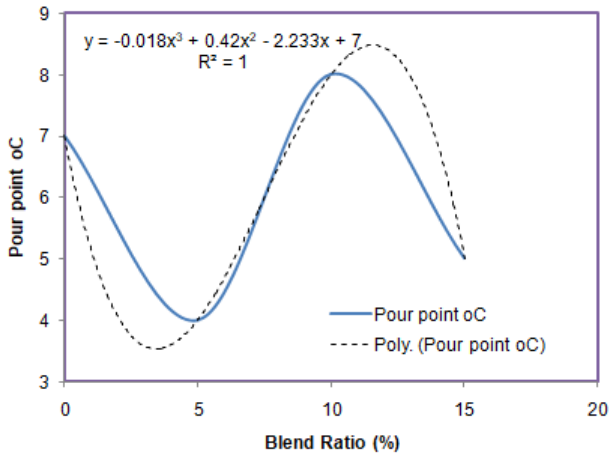

Figure 10: Trend of Pour point oC versus Blend Ratio (%)

The cetane number and blending ratios are shown in Figure 11. The Cetane number of the fuel combination varies from 0% to 15%, peaking at 15°C at a 10% blend ratio. Higher octane and lower cetane of ethanol affect blend cetane. At ethanol concentrations of 0–5%, the combination behaves like gasoline; at 5–10%, ethanol and gasoline molecules interact, raising the Cetane Number. At 10% ethanol, the mix has the maximum Cetane Number, indicating optimal amalgamation. A higher Cetane Number improves gasoline ignition and reduces engine knocking, and optimum blending ratios reduce emissions and efficiently burn fuel.

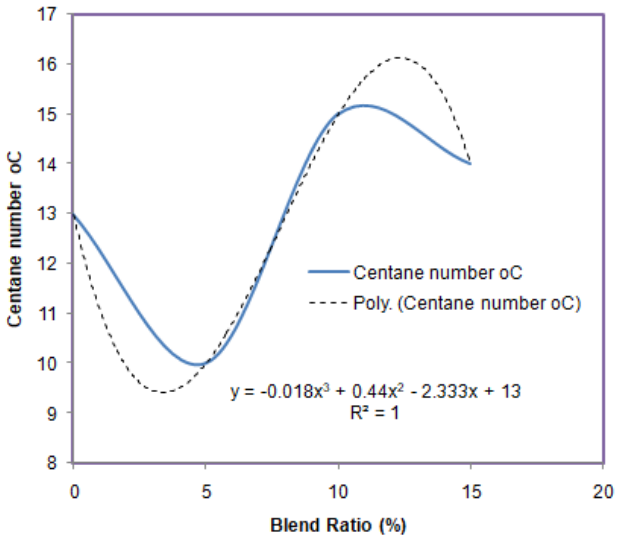

Figure 11: Trend of Cetane number oC versus Blend Ratio (%)

Characterization of Engine Test ResultsforE0, E5, E10 and E15 Blends

Speed, torque, braking power, brake thermal efficiency, and COP from the four-stroke spark-ignition engine test rig. Results are shown in Figures 12-14. The finding was used to determine the engine test rig's gasoline-bioethanol performance parameters. Figure 12 shows torque (Nm), Figure 13 shows braking power (kW), and Figure 14 shows brake thermal efficiency (%) and COP from the engine test rig running on a gasoline-bioethanol blend at 356.19 rad/sec. Analyzing engine performance data at 356.19 rps while adjusting torque, braking power, and brake thermal efficiency.

Figure 12 shows that torque (Nm) declines with the gasoline-bioethanol ratio. Lower torque reduces engine power and performance, but lower energy density and changed combustion characteristics may reduce fuel efficiency and impair acceleration and responsiveness.

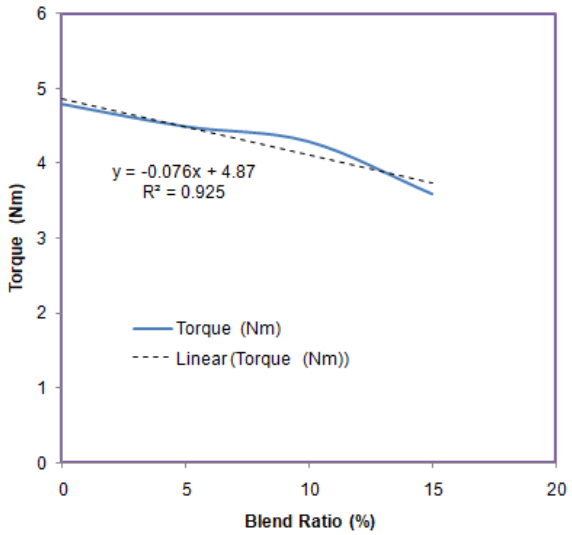

Figure 12: Trend of Torque (Nm) versus Blend Ratio (%)

Figure 13 shows how the gasoline-to-bioethanol blend ratio affects brake power (kW). Brake Power (kW) decreases non-linearly with the bioethanol mix ratio, with a greater loss at higher bioethanol concentrations. Bioethanol's lower energy content reduces brake power and bioethanol's high octane rating can cause engine knock or pinging, reducing brake power and fuel efficiency. Low Brake Power reduces vehicle acceleration, responsiveness, and performance, lowers fuel efficiency, especially at high bioethanol mix ratios, and damages engine components over time.

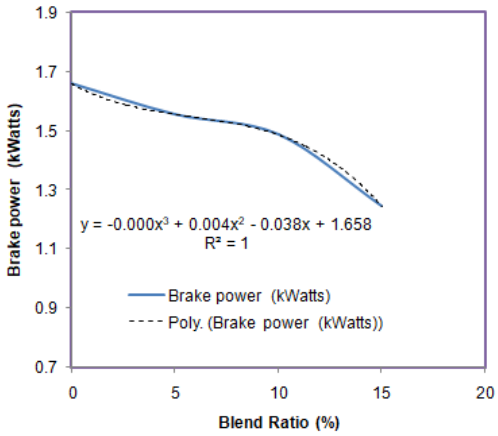

Figure 13: Trend of Brake power (kW) versus Blend Ratio (%)

Figure 14 shows that the gasoline-to-bioethanol blend ratio linearly decreases braking power efficiency. The coefficient of performance (COP) declines from 0% to 10% as the gasoline-to-bioethanol blend ratio increases, but 12% remains stable beyond 10%. Braking power efficiency decreases linearly with the bioethanol mix ratio, therefore each percentage point increase in bioethanol reduces this efficiency. As the bioethanol blend ratio increases from 0% to 10%, the coefficient of performance (COP) decreases, but it stabilizes at 6% above 10%. Bioethanol requires engines to adjust to their combustion properties at high mix percentages and blends above 10% increase performance and reduce losses. High bioethanol concentrations increased combustion efficiency, compensating for energy density decreases, although the long-term effects on engine components need to be assessed. The brake power of the E10 gasoline-bioethanol blend peaks at 391.65 W, which is the engine's output power after friction and other losses. The E10 gasoline-bioethanol combination (8.16%) has higher brake power, indicating a more efficient engine at the same speed.

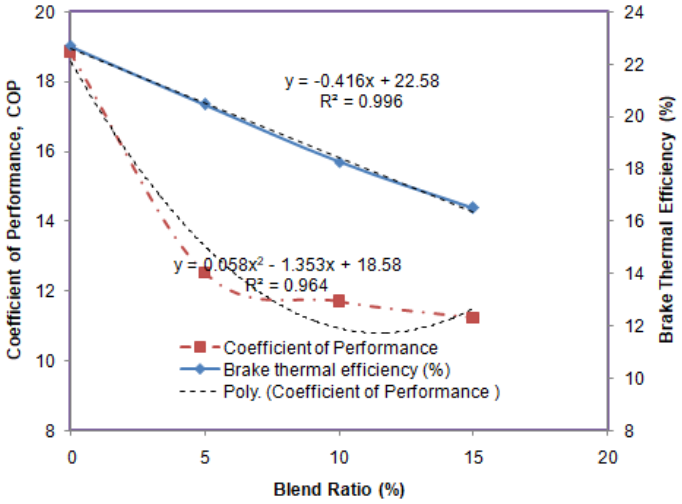

Figure 14: Trend of braking thermal efficiency and Coefficient of Performance (COP) of the system versus Blend Ratio (%)

Table 1.0 presents a summary of the predictive model with R^2 and calculated values of RSME as displayed in the Figures 4 -14 .RMSE quantifies the disparity between predicted and actual values of the trends as depicted in the Figures 4 -14. It computes the square root of the mean of the squared deviations between expected and actual values. Low RMSE values signify that the model effectively fits the data and yields more precise forecasts, whereas high RMSE values denote greater inaccuracy and reduced forecasting precision. RMSE values ranging from 0.2 to 0.5 indicate that the model can predict data with acceptable accuracy, whereas lower values signify superior model fit and enhanced prediction accuracy. Adjusted R-squared quantifies the proportion of variance in the dependent variable elucidated by the independent variables, with elevated Adjusted R-squared values signifying a high degree of precision. Criteria for modified R-squared values A value of 0.75 or above signifies a high degree of accuracy, while a value of 0.4 or higher is considered acceptable in some circumstances. RMSE and R-squared serve as complementing metrics for assessing model performance. RMSE quantifies the discrepancy between predicted and actual values of the parameters, whereas Adjusted R-squared assesses the fraction of variance elucidated by the model.

Table 1.0 Summary of the predictive model with R-squared and RSME

Properties	**Model for Blend Ratio (0%-15%)**	**Coefficient of Determination**	**RMSE**
Octane Number	$y = -0.012x^3 + 0.36x^2 - 2.683x + 14$	$R^2 = 1$	**1.176982**
Viscosity	$y = 0.003x^3 - 0.082x^2 + 0.531x + 0.411$	$R^2 = 1$	**0.27155743**
Flashpoint	$y = -0.018x^3 + 0.54x^2 - 3.733x + 32$	$R^2 = 1$	**1.176982**
Density	$y = 1E\text{-}04x^3 - 0.003x^2 + 0.024x + 0.835$	$R^2 = 1$	**0.041391**
Carbon Residue %	$y = 0.13x^2 - 2.13x + 83.35$	$R^2 = 0.949$	**0.782624**
Specific Gravity	$y = -0.002x^2 + 0.016x + 0.829$	$R^2 = 0.995$	**0.076575**
Pour point	$y = -0.018x^3 + 0.42x^2 - 2.233x + 7$	$R^2 = 1$	**1.176982**
Cetane number	$y = -0.018x^3 + 0.44x^2 - 2.333x + 13$	$R^2 = 1$	**1.176982**
Torque	$y = -0.076x + 4.87$	$R^2 = 0.925$	**0.533772**
Brake power	$y = -0.000x^3 + 0.004x^2 - 0.038x + 1.658$	$R^2 = 1$	**0.384199**
Braking thermal efficiency	$y = -0.416x + 22.58$	$R^2 = 0.996$	**0.132853**
Coefficient of Performance (COP)	$y = 0.058x^2 - 1.353x + 18.58$	$R^2 = 0.964$	**0.585587**

Low RMSE values indicate that the model effectively fits the data and generates more precise predictions. Conversely, increased values suggest a decrease in forecast accuracy and a greater degree of inaccuracy. The R-squared is a standardized equivalent of the root mean square error, which is a non-standardized measure of goodness-of-fit. The majority of the models in Table 1.0 have RMSE values ranging from 0.2 to 0.5, which indicates that the model can predict the data with reasonable accuracy. Additionally, an R-squared value of 0.75 or higher indicates a high level of accuracy, according to a general guideline. The

RMSE and R-squared values of the Coefficient of Performance (COP) are 0.585587 and 0.964, respectively. The RMSE and R-squared of the braking thermal efficiency are 0.132853 and 0.996, respectively.

V. CONCLUSIONS

The following conclusions were derived from the present investigation on an evaluation of predictive modeling and error analysis for physicochemical characteristics of gasoline-bioethanol blends in a gasoline engine. The results revealed that bioethanol significantly influences the engine's performance metrics. The coefficient of performance (COP) displayed high sensitivity to bioethanol content in the 0-10% range and stabilized beyond 10%, indicating an optimal blend ratio around E10. While brake power efficiency decreased linearly with increasing bioethanol content due to its lower energy density, enhanced combustion efficiency at higher ethanol ratios mitigated these losses. The E10 blend emerged as the most practical and efficient option, achieving the highest brake power of 391.65 W.

The predictive models developed in this study demonstrated strong accuracy, with R-squared values of 0.964 for COP and 0.996 for braking thermal efficiency, alongside RMSE values of 0.585 and 0.133, respectively. These metrics validate the reliability of the models in predicting engine performance across varying blend ratios. The findings emphasize the E10 blend as an optimal solution for balancing engine performance and environmental benefits. This study contributes to the growing body of research on bioethanol-gasoline blends and highlights the potential for their broader application in sustainable energy systems.

Conflicts of Interest

The authors declare no conflicts of interest.

REFERENCES

[1]. Su, Y.; Zhang, P.; Su, Y. An Overview of Biofuels Policies and Industrialization in the Major Biofuel Producing Countries. Renew. Sustain. Energy Rev. **2015**, 50, 991–1003

[2]. De Souza, T.A.Z.; Pinto, G.M.; Julio, A.A.V.; Coronado, C.J.R.; Perez-Herrera, R.; Siqueira, B.O.P.S.; da Costa, R.B.R.; Roberts, J.J.; Palacio, J.C.E. Biodiesel in South American Countries: A Review on Policies, Stages of Development and Imminent Competition with Hydrotreated Vegetable Oil. Renew. Sustain. Energy Rev. **2022**, 153, 111755.

[3]. Giakoumis, E.G.; Dimaratos, A.M.; Rakopoulos, C.D.; Rakopoulos, D.C. Combustion Instability during Starting of Turbocharged Diesel Engine Including Biofuel Effects. J. Energy Eng. **2017**, 143, 4016047.

[4]. Setiawan, I.C.; Setiyo, M. Renewable and Sustainable Green Diesel (D100) for Achieving Net Zero Emission in Indonesia Transportation Sector. Automot. Exp. **2022**, 5, 1–2.

[5]. Maawa, W.N.; Mamat, R.; Najafi, G.; De Goey, L.P.H. Performance, Combustion, and Emission Characteristics of a CI Engine Fueled with Emulsified Diesel-Biodiesel Blends at Different Water Contents. Fuel **2020**, 267, 117265

[6]. Giakoumis, E.G.; Rakopoulos, C.D.; Dimaratos, A.M.; Rakopoulos, D.C. Combustion Noise Radiation during the Acceleration of a Turbocharged Diesel Engine Operating with Biodiesel or N-Butanol Diesel Fuel Blends. Proc. Inst. Mech. Eng. Part D J. Automob. Eng. **2012**, 226, 971–986

[7]. Khan, I.U. Analysis of Biodiesel and Fatty Acids Using State-of-the-Art Methods from Non-Edible Plants Seed Oil; Nicotiana Tobaccum and Olea Ferruginia. Process Saf. Environ. Prot. **2024**, 186, 25–36.

[8]. Krishnasamy, A.; Bukkarapu, K.R. A Comprehensive Review of Biodiesel Property Prediction Models for Combustion Modeling Studies. Fuel **2021**, 302, 121085

[9]. Palani, Y.; Devarajan, C.; Manickam, D.; Thanikodi, S. Performance and Emission Characteristics of Biodiesel-Blend in Diesel Engine: A Review. Environ. Eng. Res. **2022**, 27, 200338.

[10]. Bukkarapu, K.R.; Krishnasamy, A. A Critical Review on Available Models to Predict Engine Fuel Properties of Biodiesel. Renew. Sustain. Energy Rev. **2022**, 155, 111925

[11]. Suvarna, M.; Jahirul, M.I.; Aaron-Yeap, W.H.; Augustine, C.V.; Umesh, A.; Rasul, M.G.; Günay, M.E.; Yildirim, R.; Janaun, J. Predicting Biodiesel Properties and Its Optimal Fatty Acid Profile via Explainable Machine Learning. Renew. Energy **2022**, 189, 245–258

[12]. Xiao, H.; Wang, W.; Bao, H.; Li, F.; Zhou, L. Biodiesel-Diesel Blend Optimized via Leave-One Cross-Validation Based on Kinematic Viscosity, Calorific Value, and Flash Point. Ind. Crops Prod. **2023**, 191, 115914

[13]. Sangotayo E.O, Nnamchi S.N., Mundu M.M. and Ibrahim K. (2023) Modeling of the Operational Parameters on the Performance of an Air Conditioning System, IDOSR Journal of Experimental Sciences 9(2) pp.135-148,

[14]. Yusoff, M.N.A.M.; Zulkifli, N.W.M.; Sukiman, N.L.; Chyuan, O.H.; Hassan, M.H.; Hasnul, M.H.; Zulkifli, M.S.A.; Abbas, M.M.; Zakaria, M.Z. Sustainability of Palm Biodiesel in Transportation: A Review on Biofuel Standard, Policy and International Collaboration Between Malaysia and Colombia. Bioenerg. Res. **2021**, 14, 43–60.

[15]. Gebremariam, S.N.; Marchetti, J.M. Economics of Biodiesel Production: Review. Energy Convers. Manag. **2018**, 168, 74–84.

[16]. Filho, E.P.M., Oliveira, A.P., Vita, W.A., Mesquita, F.L.L., Codato, G., Escobedo, J.F., Cassol, M. and Franca, J.R.A. (2016) Global, Diffuse and Direct Solar Radiation at the Surface in the City of Rio de Janeiro: Observational Characterization and Empirical Modeling. Renewable Energy, 91, 64-74

[17]. Despotovic, M., Nedic, V., Despotovic, D. and Cvetanovic, S. (2016) Evaluation of Empirical Models for Predicting Monthly Mean Horizontal Diffuse Solar Radiation. Renewable and Sustainable Energy Reviews, 56, 246-260.

[18]. Bailek, N., Bouchouicha, K., Al-Mostafa, Z., El-Shimy, M., Aoun, N., Slimani, A. and Al-Shehri, S. (2018) A New Empirical Model for Forecasting the Diffuse Solar Radiation over Sahara in the Algerian Big South. Renewable Energy, 117, 530-537.

[19]. Khalil, S.A. and Shaffie, A.M. (2013) A Comparative Study of Total, Direct, and Diffuse Solar Irradiance by Using Different Models on Horizontal and Inclined Surfaces for Cairo, Egypt. Renewable and Sustainable Energy Reviews, 27, 853-863

[20]. Akpootu, D. O., & Iliyasu, M. I. (2015). A comparative study of some meteorological parameters for predicting global solar radiation in Kano, Nigeria based on three variable correlations. Advances in Physics Theories and Applications, 49, 1–9.